European Journal of Lipid Science and Technology

WILEY-VCH

European Journal of
Lipid Science and Technology

RESEARCH ARTICLE OPEN ACCESS

Pushing Poly(Limonene Carbonate) Toward Commercial Applications: Bio-Based Poly(Menth-1-Ene Carbonate)-*Graft*-Poly(*n*-Butyl Acrylate) With Tailored Graft Density

Marcel Höferth | Holger Schmalz | Andreas Greiner

Macromolecular Chemistry and Bavarian Polymer Institute, University of Bayreuth, Bayreuth, Germany

Correspondence: Andreas Greiner (andreas.greiner@uni-bayreuth.de)

Received: 8 February 2025 | **Revised:** 2 April 2025 | **Accepted:** 20 May 2025

Funding: Financial support was provided by the German Research Foundation (DFG, GR 972/59-1).

Keywords: bio-based | compatibilization | graft | polycarbonate | toughening

ABSTRACT

Poly(limonene carbonate) (PLimC) is a promising material in the search for bio-based alternatives to fossil-based plastics, such as poly(styrene) and bisphenol A-based polycarbonates. PLimC is made from orange waste-derived limonene oxide (LimO) and CO_2. The brittle behavior of PLimC remains a challenge for industrial applications. A possible solution could be the introduction of low T_g polymer grafts. The terpolymerization of *trans*-LimO, *trans*-menth-1-ene oxide (Men1O), and CO_2 was shown to yield a terpolymer that can be used as a platform for controlled functionalization and tailored graft copolymerization. To transform the terpolymer into a macroinitiator for atom transfer radical polymerization (ATRP), the PLimC double bonds were post-modified with hydroxyl groups via thiol-ene click reaction of 2-mercaptoethanol and subsequently esterified with 2-bromoisobutyryl bromide (BiB). *n*-Butyl acrylate (*n*BA) was chosen as a bio-based monomer for grafting-from copolymerization to introduce low T_g side chains that increase the ductility of the otherwise brittle PLimC. Matrix-assisted laser desorption ionization time-of-flight mass spectrometry (MALDI-TOF MS) was used to show the narrow molecular weight distribution of the side chains. Non-wovens made from PMen1C-*g*-P*n*BA were produced via electrospinning. PMen1C-*g*-P*n*BA was added as a compatibilizer for blends of PLimC and poly(*n*-butyl acrylate) (P*n*BA) and as a toughening agent for PLimC.

Practical Applications: PMen1C-*g*-P*n*BA shows tunable mechanical properties by variation of P*n*BA content and graft density. Poly(limonene carbonate)'s brittle nature could be compensated by addition of PMen1C-*g*-P*n*BA, therefore opening up many possible industrial applications for PLimC to replace common fossil-based plastics. Additionally, filter applications of PMen1C-*g*-P*n*BA as sustainable electrospun non-wovens are possible.

ATRP, atom transfer radical polymerization; DSC, differential scanning calorimetry; ^{1}H NMR, proton nuclear magnetic resonance; MALDI, matrix-assisted laser-desorption/ionization; PLimC, poly(limonene carbonate); PMen1C, poly(menth-1-ene carbonate); P*n*BA, poly(*n*-butyl acrylate); SEC, size exclusion chromatography; TGA, thermogravimetric analysis.

1 | Introduction

For the last few decades, there has been an increasing interest in environmentally friendly and non-fossil-based polymer materials. Among these, bio-based polymers have gained considerable interest due to their potential to replace their fossil-based counterparts and reduce the environmental impact associated with traditional polymer production [1–5]. A prominent example of a bio-based, non-food-derived raw material is *R*-(+)-limonene. It can be extracted from orange peels and converted into polymers such as polyamides, polyurethanes, and polycarbonates in a variety of ways [6, 7]. Notably, one such polymer is poly(limonene carbonate) (PLimC), which is synthesized by copolymerization of limonene oxide (LimO) and carbon dioxide (CO_2) using a β-diiminato-zinc catalyst [8–11]. PLimC exhibits exceptional transparency and hardness, surpassing that of conventional bisphenol A (BPA)-based polycarbonate. Additionally, its remarkable gas permeability and selectivity toward CO_2 make it a promising candidate for bio-based "breathing glass" applications [12]. The ability to chemically recycle PLimC back into the LimO monomer, combined with favorable life cycle assessments, highlights its potential for integration into circular economy frameworks [13–15]. Furthermore, the exocyclic double bond in PLimC offers opportunities for post-polymerization modifications, expanding its versatility [16–18]. Like most other aliphatic polycarbonates obtained from epoxides and CO_2, PLimC shows poor mechanical and thermal properties compared to BPA-based polycarbonates. Although the tensile strength (50 MPa) is sufficiently high (comparable to poly(ethylene terephthalate) (55 MPa)) [19], the low elongation at break (ca. 5%, similar to poly(styrene) [20]) makes it too brittle for most commercial products. Additionally, the gap between the thermal decomposition temperature ($T_{5\%}$ = 225°C, where $T_{5\%}$ is the temperature at 5% weight loss) to its glass transition temperature (T_g = 130°C) is too narrow, and its melt viscosity is comparably high, limiting most processing technologies, such as injection molding and extrusion [9].

A major challenge in the utility of PLimC for industrial applications is therefore improving these properties, while conserving the beneficial properties. Plasticizers have already been shown to decrease the brittleness and improve the processability of PLimC [21]. However, the addition of small molecules such as the used ethyl oleate decreased the tensile strength and Young's modulus and is expected to cause migration to the surface and leaching, leading to embrittlement and contamination [22, 23].

Branched plasticizers could be the solution to these problems [23]. Polymers with a branched architecture are known to be less brittle than their linear counterpart because the entropic constraints of the side chains can allow the chains to flow, leading to plastic deformation and a ductile break [24–26]. Matyjaszewski et al. even demonstrated densely-grafted graft copolymers as super soft elastomers [27, 28]. Graft copolymers also have proven useful to counteract brittleness as additives to a miscible polymer matrix like PLLA [29]. The application of graft copolymers as compatibilizers [30–40], toughening agents [29, 41], and plasticizers [42] has been researched for many years. In the case of PLimC, grafting from polymerization after complete functionalization, however, leads to a bottlebrush-type polymer, in which a side chain is grown from every single repeating unit (Scheme 1).

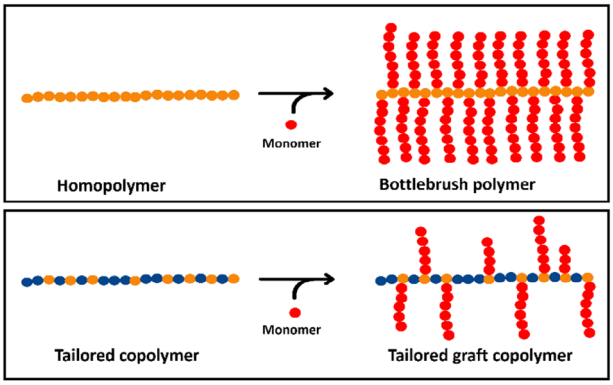

SCHEME 1 | In a grafting-from polymerization with completely functionalized PLimC, a side chain is grown from every single repeating unit, creating a bottlebrush-type conformation. The numbers of repeating units of the grafted polymer outweigh the backbone polymer.

The result would be high molecular weights, even with relatively short side chains, a more rod-like conformation [43], and a much higher content of the grafting polymer than the PLimC backbone [44, 45].

The graft density has been tailored by various methods in the past [46–54]. One possibility to adjust the graft density would be to synthesize copolymers, which implement one repeating unit that acts as an initiation site for grafting from polymerization, while the other repeating unit stays inert. This copolymer would need to have a random composition for an equal distribution of the grafted side chains on the main polymer chain. Frey et al. established the terpolymerization of propylene oxide with 1,2-epoxy-5-hexene and CO_2, which were subsequently functionalized with 2-mercaptoethanol, yielding macroinitiators for the ring-opening polymerization of L-lactide [55]. Our group previously demonstrated the synthesis of random copolymers of PLimC through the terpolymerization of LO, its hydrogenated counterpart menthene oxide (Men1O), and CO_2 [56]. The functionalization of these terpolycarbonates via thiol-ene click chemistry with 2-mercaptoethanol was also established, yielding hydroxyl-functionalized polymers. Building on this prior work, we now report the conversion of these bio-based terpolycarbonates into graft copolymers with precisely tailored graft densities.

To achieve controlled side chain growth, atom transfer radical polymerization (ATRP) was employed. Hydroxyl groups on the terpolymers were functionalized with 2-bromoisobutyryl bromide (BiB) to create ATRP initiation sites. *n*-Butyl acrylate (*n*BA) was selected as the comonomer for grafting due to its well-documented behavior in controlled radical polymerizations and the favorable mechanical properties of its resulting polymer, poly(*n*-butyl acrylate) (P*n*BA) [57–61]. P*n*BA side chains were introduced to address the inherent brittleness of PLimC, enhancing the ductility of the polymer system. Notably, the potential for bio-based synthesis of *n*BA has been demonstrated, further aligning this work with principles of sustainability [62–64].

We investigated the material properties of PMen1C-*g*-P*n*BA graft copolymers with varying graft densities and graft chain lengths. The graft copolymers were evaluated as electrospun non-woven mats and as compatibilizers for immiscible PLimC/P*n*BA blends. Moreover, the mechanical properties of PLimC were compared to those of PLimC toughened with PMen1C-*g*-P*n*BA, demonstrating the effectiveness of the graft copolymer as a toughening agent. The novelty of this work lies in the combination of a bio-based, non-food-based polycarbonate backbone with a controlled grafting strategy and the exploration of multiple practical applications, presenting a versatile and sustainable approach to enhancing polymer material performance of PLimC.

2 | Materials and Methods

The monomers *trans*-LimO and *trans*-Men1O, along with the catalyst [(BDI)Zn-μOAc], were synthesized following established literature protocols [9, 10]. Gas chromatography (GC) analysis determined the purity of LimO and 1-MenO to be 84% and 92% in the *trans*-conformation, respectively. The copolymers PMen1C-*ran*-PLimC were prepared as described previously [56].

2-Mercaptoethanol (99%) was obtained from Carl Roth. Azobisisobutyronitrile (AIBN) was sourced from Sigma-Aldrich and purified by recrystallization from methanol. Copper(I) bromide (CuBr; 98%), copper(II) bromide ($CuBr_2$; 99%), BiB (98%), *N,N,N′,N″,N″*-pentamethyldiethylenetriamine (PMDTA; 99%), and 1,5,7-triazabicyclo[4.4.0]dec-5-ene (TBD; 98%) were also purchased from Sigma-Aldrich.

nBA (98+%, stabilized with 50 ppm 4-methoxyphenol), ethyl 2-bromoisobutyrate (EBiB), and basic aluminum oxide (AlOx) were obtained from Thermo Scientific. Triethylamine (TEA; 99%) was supplied by Grüssing. P*n*BA solution ($\bar{M}_{n,\,app} = 105$ kg mol^{-1}) was purchased from Alfa Aesar. Solvents including acetone, chloroform ($CHCl_3$), methanol (MeOH), and ethyl acetate (technical grade) were purified by distillation.

PLimC ($\bar{M}_{n,\,app}$ = 96 kg mol^{-1}), used in blend films, was synthesized previously according to literature methods [9].

2.1 | Synthesis of Macroinitiator PMen1C-BiB

The procedures were adapted from literature and are exemplarily described for a random terpolymer with 10 mol% LimC repeating units [9, 16, 56]. P(Men1C-*ran*-LimC) (15.0 g, 10 mol% (7.58 mmol) LimC repeating units) was dissolved in 250 mL chloroform. An amount of 373 mg AIBN (2.27 mmol, 0.3 equiv.) and a volume of 16.0 mL 2-mercaptoethanol (227.4 mmol, 30 equiv.) were added and heated under reflux for 24 h. The polymer was then precipitated in methanol and dried under reduced pressure at 80°C.

P1MenC-OH (8.0 g; 10 mol% (3.85 mmol) OH groups; 1 equiv.) was dissolved in 140 mL chloroform. A volume of 610 µL TEA (4.62 mmol; 1.2 equiv.) and 571 µL BiB (4.62 mmol; 1.2 equiv.) were added at 0°C and stirred for 24 h. The polymer was then precipitated in methanol and dried in rotary vane pump vacuum at 80°C. The resulting polymer was analyzed by proton nuclear magnetic resonance (^{1}H NMR) spectroscopy and size exclusion chromatography (SEC).

2.2 | ATRP of *n*BA Homopolymer

The reaction conditions for the graft copolymerization of P*n*BA onto PMenC-BiB via ATRP were adapted according to literature procedures and tested with EBiB as initiator [61]. An amount of 119 mg CuBr (0.83 mmol; 1 equiv.) was added to a 25 mL Schlenk flask and dissolved in 2.4 mL degassed acetone with 173 µL PMDTA (0.83 mmol; 1 equiv.). *n*BA was destabilized by passing over basic AlOx and degassed by argon bubbling. A volume of 12 mL *n*BA (83.3 mmol; 100 equiv.) was added to the solution and stirred, while degassing by argon bubbling. The initiator EBiB (108 µL; 0.83 mmol; 1 equiv.) was added to the solution, the Schlenk flask was sealed with a rubber septum, and the mixture was stirred at 60°C. Samples were drawn after 0, 1 h, and so forth, to monitor conversion of *n*BA. Monomer conversion reached over 50% after 2 h, so the reaction was stopped by opening the Schlenk flask. After cooling to 0°C, the green solution was filtered over AlOx to remove the catalyst, then precipitated in a methanol-water-mixture (70:30, v/v). The turbid supernatant was discarded, and the viscous polymer at the bottom of the beaker was dried at 70°C in rotary vane pump vacuum. The resulting polymer was analyzed by ^{1}H NMR spectroscopy and SEC.

2.3 | Synthesis of PMen1C-*g*-P*n*BA

As an example, PMen1C-BiB (1.71 g; 10 mol% (0.83 mmol) BiB moieties; 1 equiv.) was added to a 50 mL Schlenk flask. An amount of 119 mg CuBr (0.83 mmol; 1 equiv.) was added to a 25 mL Schlenk flask and dissolved in 2.4 mL degassed acetone with 173 µL PMDTA (0.83 mmol; 1 equiv.). *n*BA was destabilized by passing over basic AlOx and degassed by argon bubbling. A volume of 12 mL *n*BA (83.3 mmol; 100 equiv.) was added to the macroinitiator and stirred to dissolve, while degassing by argon bubbling. The CuBr/PMDTA-complex solution was added to the macroinitiator, and the mixture was stirred at 60°C. Samples were drawn after 0, 1 h, and so forth, to monitor conversion of *n*BA *via* ^{1}H NMR spectroscopy. Monomer conversion reached over 50% after 5 h, so the reaction was stopped by opening the Schlenk flask. After cooling to 0°C, the green viscous solution was diluted with acetone and filtered over AlOx to remove the catalyst, then precipitated in methanol and dried at 70°C in rotary vane pump vacuum. The resulting polymer was analyzed by ^{1}H NMR spectroscopy and SEC.

2.4 | Cleavage of P*n*BA Side Chains

The cleavage of P*n*BA side chains was performed analogously to the procedure for base-initiated depolymerization of PLimC [13]. PMen1C-*g*-P*n*BA (200 mg; 0.04 mmol carbonate repeating units) and TBD (60 mg) were added to a 75 mL glass pressure tube and dissolved in 25 mL dry toluene, and the mixture was stirred at 110°C for 20 h. The toluene was then partially removed by rotary evaporation, and the resulting mixture was precipitated in a methanol/water mixture (7:3, v/v) and stored at 4°C for 16–18 h. After decanting the supernatant, the P*n*BA was dried in rotary

TABLE 1 | Graft copolymerization of *n*BA onto PMen1C-BiB backbone.

Entry	Graft density[a] (mol%)	$\bar{M}_{n,\,app,MI}$[b] (kg mol^{-1})	$\bar{M}_{n,\,app,GP}$[b] (kg mol^{-1})	P*n*BA content[a] (mol%)
1	4	99	162	66
2	7	78	86	39
3	10	70	100	72
4	10	70	129	77
5	20	80	264	83
6	33	87	328	98

[a]Calculated using ^{1}H NMR spectroscopy (300 MHz, $CDCl_3$).
[b]Apparent number-averaged molecular weight ($\bar{M}_{n,\,app}$) measured by $CHCl_3$-SEC (PS calibration).

vane pump vacuum at 60°C for 16–18 h and investigated using SEC, ^{1}H NMR spectroscopy, and matrix-assisted laser desorption ionization time-of-flight mass spectrometry (MALDI-TOF MS).

2.5 | Solvent Casting and Mechanical Analyses

The graft copolymers, as well as the PLimC blends, were cast into films by dissolving 1.3 g of the respective polymer in 20 mL of dichloromethane and pouring the solutions into glass petri dishes ($Ø$ = 8 cm), followed by slowly drying at 25°C for 96 h and subsequently in a rotary vane pump vacuum for at least 24 h. The specimens then were left in the testing laboratory for 24 h to acclimatize.

For mechanical analyses, the films were cut into rectangles (3 cm × 3 mm), and the thickness was measured with a Mitutoyo Quick-Mini Digital Thickness Gauge. Afterward, the films were clamped into a ZwickRoell BTI-FRO.5TN.D14 tensile tester equipped with a 200 N load cell and tested at a speed of 10 mm min^{-1}.

2.6 | Electrospinning of PMen1C-*g*-P*n*BA

The 20, 30, and 40 wt% solutions of PMen1C-$g_{10\%}$-P*n*BA (Table 1, Entry 3) in $CHCl_3$ were prepared. Fiber mats were spun with a voltage of −2 to 15 kV at 20 cm distance for 10 min onto a flat aluminum foil at a flow rate of up to 2 mL h^{-1}. The flow rate was induced with a syringe pump (Landgraf Laborsysteme LA-100), and the solution was extruded through a 1 mL syringe and a 0.4 × 25 mm cannula with a blunt tip.

2.7 | Atomic Force Microscopy (AFM)

AFM measurements were performed on a Bruker Icon 2 with a Cantilever (Olympus) at a scan rate of 0.5 Hz in tapping mode and height mode. The samples were prepared by spin-coating of a 1 mg mL^{-1} solution of PMen1C-$g_{10\%}$-P*n*BA (Table 1, Entry 3) in ethyl acetate onto a cleaned silicon wafer piece.

2.8 | Methods

NMR spectra were acquired using a Bruker Avance-300 NMR spectrometer operating at 300 MHz, with deuterated chloroform ($CDCl_3$) as the solvent. Chemical shifts (δ) are reported in parts per million (ppm) relative to the residual solvent signals. MALDI-TOF mass spectra were obtained using a Bruker Autoflex maX in linear mode. The matrix used was *trans*-2-[3-(4-tert-butylphenyl)-2-methyl-2-propenylidene]malononitrile (DCTB) dissolved in THF, with sodium trifluoroacetate (10 g L^{-1}) serving as the ionizing agent (matrix/sample/ionizing agent ratio: 20:3:1).

Differential scanning calorimetry (DSC) measurements were performed on a Netzsch 204 F1 Phoenix system at a scanning rate of 10°C min^{-1} under a nitrogen atmosphere. Thermogravimetric analysis (TGA) was conducted using a Netzsch TG 209 F1 Libra, also at a scanning rate of 10 K min^{-1} under a nitrogen atmosphere.

SEC analyses were carried out on an Agilent 1200 system equipped with an SDV pre-column (particle size 5 µm, PSS Mainz), an SDV linear XL column (particle size 5 µm, PSS Mainz), and a refractive index detector (G1362A, Agilent Technologies). HPLC-grade chloroform ($CHCl_3$) was used as the mobile phase at a flow rate of 0.5 mL min^{-1} at room temperature. Calibration was performed with narrowly distributed polystyrene standards (PSS calibration kit), and HPLC-grade toluene was used as the internal standard.

Raman imaging was conducted using a WITec Alpha 300 RA+ Raman AFM microscope.

3 | Results and Discussion

3.1 | Synthesis of Macroinitiator PMen1C-BiB

Detailed descriptions of the syntheses are provided in Section 2. The structures as well as the composition of the functionalized terpolymers were studied by ^{1}H NMR spectroscopy (Figure 1).

The signals at 3.70 ppm (c) and 1.90 ppm (e) confirm the successful functionalization for ME and BiB, respectively, and can be used alongside the signal at 5.00 ppm (a) to calculate the content of BiB-functionalized LimC repeating units and accordingly the content of ATRP initiator groups. All functionalized terpolymers show narrow molar mass distributions and apparent number-averaged molecular weights in the range of $\bar{M}_{n,\,app} \approx$ 70–100 kg mol^{-1}, as determined by SEC. The structure and composition of the functionalized terpolymers were analyzed using ^{1}H NMR spectroscopy (Figure 1).

SEC was additionally used to confirm that the functionalization reactions did not cause degradation of the polymer backbone (Figure S1).

The measured $\bar{M}_{n,\,app}$ = 70 kg mol^{-1} for the terpolymer with 10 mol% LimC with a narrow distribution ($Đ$ = 1.12) is only shifted slightly toward higher molecular weights with the thiol-ene click functionalization reaction. These deviations can be attributed to the change in the interaction

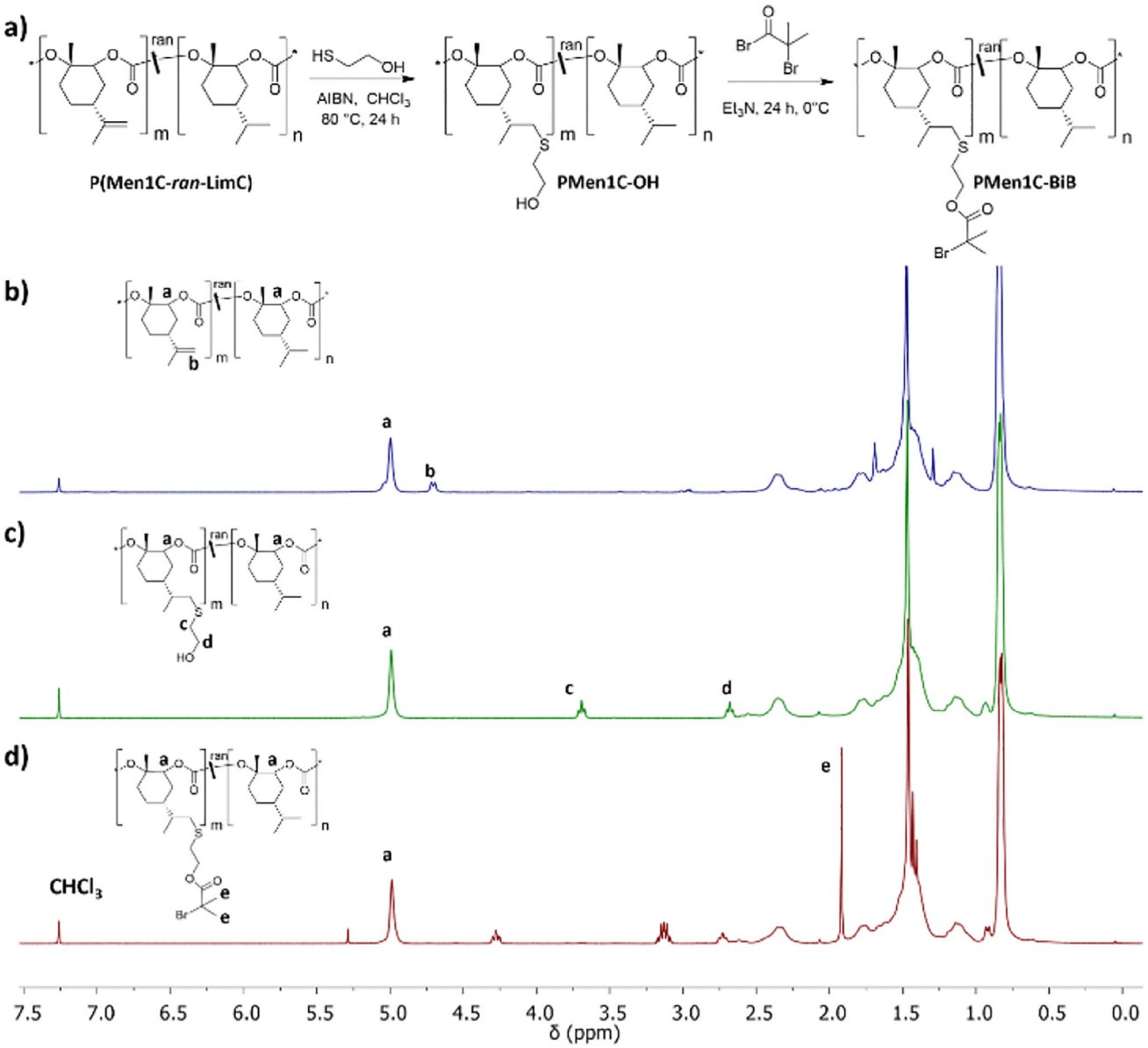

FIGURE 1 | (a) Reaction scheme of the functionalization of copolymer to macroinitiator, (b) ^{1}H NMR spectra of copolymer P(Men1C-*ran*-LimC) with 10% LimC with in $CDCl_3$, (c) NMR spectra of P(Men1C)-OH in $CDCl_3$, (d) ^{1}H NMR spectra of macroinitiator P(Men1C)-BiB in $CDCl_3$.

with solvent caused by the OH-groups and initiator groups, as well as the increase in molecular weight caused by the functionalization.

3.2 | Synthesis of PMen1C-g-P*n*BA Graft Copolymers

The reaction conditions for the ATRP of the graft copolymerization were tested beforehand by synthesizing P*n*BA homopolymers. EBiB was chosen as initiator for its similarity in structure to BiB (Scheme S1). The polymerization was performed in acetone according to literature [65, 66]. Monomer conversion of *n*BA reached 50% after 5 h, and the SEC traces showed sufficient molecular weight and narrow distribution ($\bar{M}_{n,\,app} = 5.6$ kg mol^{-1}; $Đ = 1.18$) (Figure S2).

After successful determination of the conditions for the ATRP of butyl acrylate, the graft copolymerization was performed under analogous reaction conditions, except with the PMen1C-BiB macroinitiator instead of EBiB (Scheme 2), and the structures as well as the composition of the graft copolymers were investigated using ^{1}H NMR spectroscopy and SEC (Figure 2; Figure S3; Table 1).

The spectra of the graft copolymers in Figure 2 are arranged in order of increasing grafting density, with each spectrum corresponding to its respective entry number in Table 1. With the exception of Entry 2, grafting density generally increases with the nBA content in the copolymers. Despite careful monitoring of the ATRP process using ^{1}H NMR spectroscopy and terminating the reaction at 50% conversion, the resulting graft copolymers deviated from the intended 1:1 weight ratio of nBA to Men1C repeating units, which would require an nBA molar content

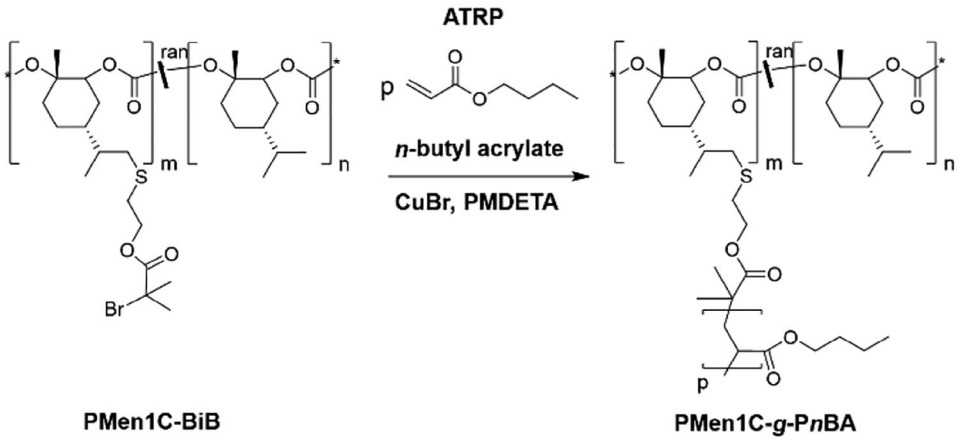

SCHEME 2 | Reaction scheme of graft copolymerization of *n*-butyl acrylate from PMen1C-BiB.

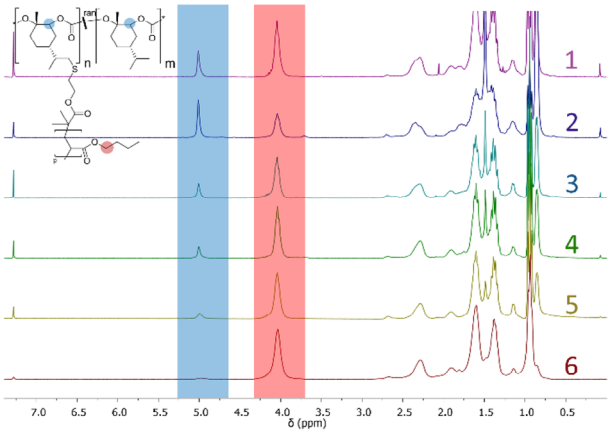

FIGURE 2 | ^{1}H NMR spectra of the PMen1C-*g*-P*n*BA graft copolymers in order of increasing graft density (see Table 1, Entries 1–6).

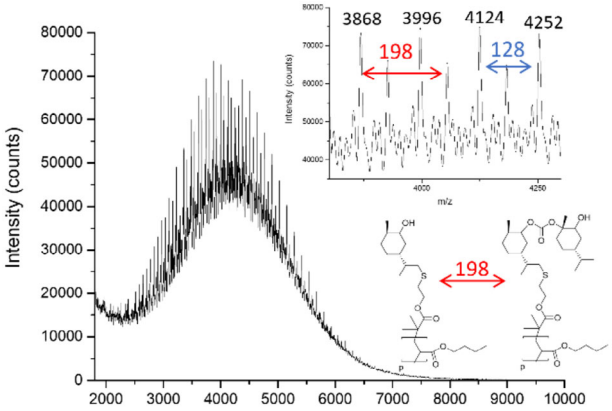

FIGURE 3 | MALDI-TOF mass spectrum of the P*n*BA side chains that were isolated from the graft copolymer by triazabicyclodecene (TBD)-catalyzed depolymerization of the polycarbonate main chain. Two series of peaks with a $\Delta m/z$ of 128.2 (*n*BA) are visible. Between the two series, the $\Delta m/z$ is 198.3, which can be assigned to one additional Men1C unit.

of approximately 64%. This ratio was targeted to optimize the study of microphase separation. As the peak of the BiB-methyl groups (2.0 ppm) should shift toward lower chemical shifts after polymerization, the remaining peak can be assumed to stem from unreacted initiator groups. In the case of PMen1C$_{28}$-g$_{10\%}$-P*n*BA$_{72}$ (3), this is the case for about 0.5 mol% of repeating units (5% of total initiator groups) (calculated by dividing the integral of peak at 2.0 ppm by 6 and then by the integral of the backbone signal at 5.0 ppm and finally dividing this by the original amount of initiator groups per repeating unit) (see Table S1). The shifted signal of the BiB-methyl groups after polymerization can unfortunately not be utilized to calculate the average chain length of the graft copolymer chains because the signal overlaps with other signals at about 1.3 ppm. Therefore, the chain length of grafted P*n*BA was exemplarily analyzed by first depolymerizing the poly(menth-1-ene carbonate) (PMen1C) main chain of PMen1C$_{28}$-g$_{10\%}$-P*n*BA$_{72}$ (3) with a published procedure and then measuring MALDI-TOF MS (Figure 3) and SEC (Figure S4) [13]. Two main series of peaks are observed that can be assigned to P*n*BA linked to one remaining Men1C repeating unit and P*n*BA linked to two remaining Men1C repeating units. The results from the MALDI-TOF MS measurement ($\bar{M}_{n,\,app}$ = 4.1 kg mol^{-1}) correlate to a side chain length of 32 *n*BA repeating units on average. SEC analysis revealed an $\bar{M}_{n,\,app}$ of 4.3 kg mol^{-1} and $Đ$ = 1.13, corresponding to an average side chain length of 33 *n*-BA repeating units with a narrow distribution. This result aligns well with the findings from the MALDI-TOF MS measurements.

SEC was also utilized to compare the macroinitiator PMen1C-BiB to the graft copolymer PMen1C-*g*-P*n*BA. This is shown exemplary for PMen1C$_{28}$-g$_{10\%}$-P*n*BA$_{72}$ (3) in Figure 4.

The molecular weight $\bar{M}_{n,\,app}$ = 70 kg mol^{-1} of the terpolymer with 10 mol% LimC with a narrow distribution ($Đ$ = 1.12) is shifted toward higher molecular weight ($\bar{M}_{n}$ = 100 kg mol^{-1}) with only a slight increase in dispersity ($Đ$ = 1.23). A higher molecular weight shoulder is detected after graft copolymerization, and especially in other examples (Figure S3) this shoulder appears more pronounced. This may be caused by crosslinking of double bonds, of which there were less than 1 mol% remaining after the functionalization reactions according to ^{1}H NMR spectroscopy. Another reason might be the occurrence of free polymerization of the *n*BA in solution after removal of the inhibitor and heating.

The thermal properties of the terpolymers were determined by TGA (Figure S5) and DSC (Figure S6). Compared to the

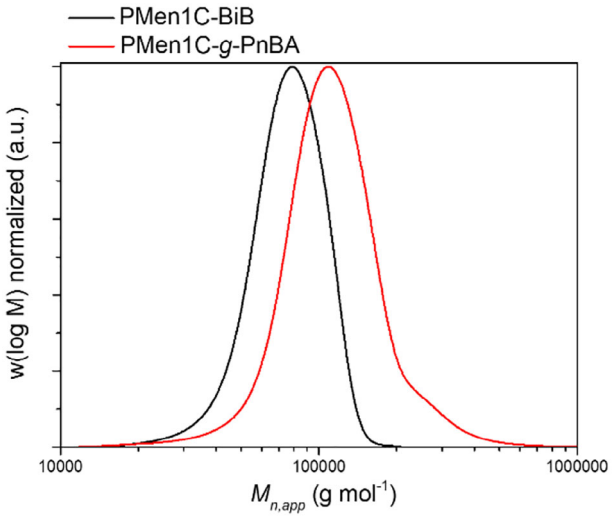

FIGURE 4 | Apparent molar mass distributions of PMen1C-BiB macroinitiator and PMen1C-*g*-P*n*BA ($CHCl_3$-SEC, PS calibration).

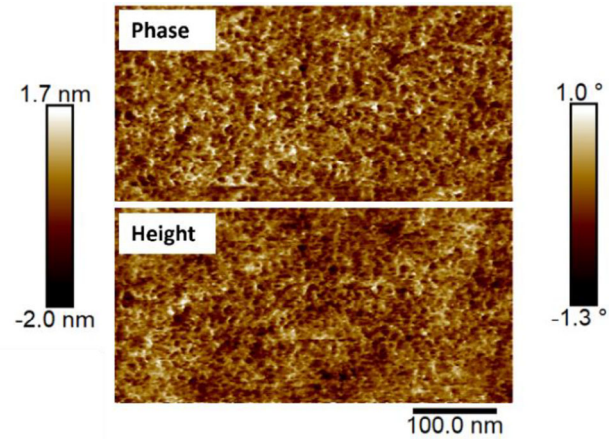

FIGURE 5 | AFM image of PMen1C$_{28}$-$g_{10\%}$-P*n*BA$_{72}$ in tapping mode shows harder softer area through phase shift.

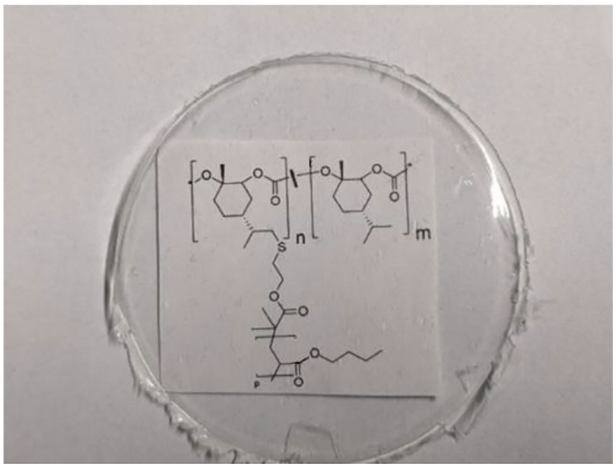

FIGURE 6 | Photographic image of PMen1C$_{28}$-$g_{10\%}$-P*n*BA$_{72}$ film, which was made by solvent casting the graft copolymer from dichloromethane.

macroinitiator PMen1C-BiB ($T_{5\%}$ = 240°C; T_g = 130°C), the thermal stability ($T_{5\%}$ = 256°C) is slightly higher, as the addition of P*n*BA (homopolymer $T_{5\%}$ = 360°C) increases the overall stability against thermal degradation except for the graft copolymers with the lowest graft densities of 4% and 7% (Table S1, Entries 1 and 2) [67]. DSC shows a trend of two T_gs, where T_{g1} is below −5°C and T_{g2} is above 72°C for the graft copolymers. The two T_gs might be the result of a partial miscibility of the backbone polymer and the grafts that shifts the T_gs toward lower or higher temperatures, respectively. However, in that case there should additionally be T_gs of the homopolymers PMen1C (T_g = 130°C) and P*n*BA (T_g = −45°C). Further thermal analysis may be necessary to clarify the influence of the graft density and graft content on the thermal behavior of the graft copolymers.

3.3 | AFM Studies

In addition, we investigated a possible microphase separation of the side chain and main chain polymers. Staining of the graft copolymers was unsuccessful because the functional groups of both PLimC and P*n*BA are too similar, leading to homogenous staining without contrast between the microphases. Therefore, TEM was not a possible method, and AFM was chosen as an alternative method for visualizing the microphase separation [68]. A thin film of PMen1C-$g_{10\%}$-P*n*BA (3) was spin-coated onto a cleaned silicon wafer piece and investigated in height mode and tapping mode (Figure 5).

As the cantilever interacts differently with the soft P*n*BA phase and stiff PMen1C phases, the resulting differences in phase shift create a contrast that visualizes the microphase separation. It is, however, uncertain if the resulting contrast in the phase image stems from the microphase separation or if it results mostly from the surface topology. The images do not clearly show patterns that are usually seen in microphase separation of copolymers. One reason might be the fact that the polymer chains of the graft copolymer are sterically much more hindered from aligning into well-defined morphologies [69]. Therefore, further investigations regarding the microphase separation might be necessary.

The influence of the graft density and graft chain length on the mechanical properties was investigated by tensile testing. For this, films of the PMen1C-*g*-P*n*BA graft copolymers were solution cast from ethyl acetate, dried and cut into specimens, then tensile tests were performed (Figures 6 and 7). Notably, the graft copolymer retains a high level of transparency, comparable to the transparency of neat PLimC. PMen1C-$g_{33\%}$-P*n*BA (6) and PMen1C-$g_{4\%}$-P*n*BA (1) could not be measured as the polymer was too soft to produce measurable specimens in the first case, and in the latter case the graft copolymerization did not yield enough material to produce specimens for the tensile tests.

It is apparent that, like neat PLimC, neat PMen1C also displays a brittle mechanical behavior. There is a clear trend visible in the stress-strain-curves that with an increasing graft density and increasing amount of *n*BA, the tensile strength and Young's modulus decrease, whereas the elongation at break increases. Zhang et al. propose that the variation in tensile toughness may

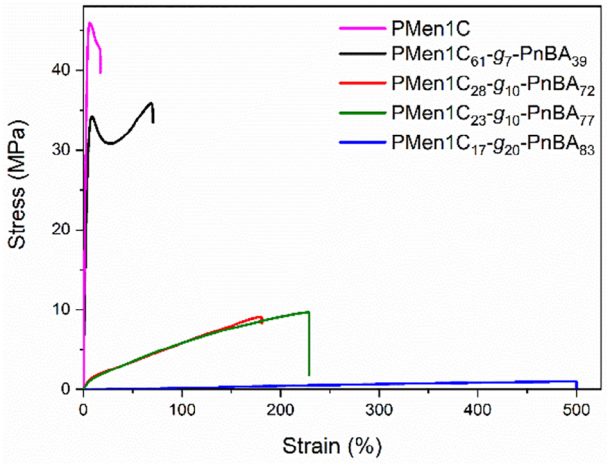

FIGURE 7 | Investigation of the mechanical behavior of samples with different side chain lengths with various compositions.

result from changes in the free volume occupied by the side chains of the graft block polymers [51]. Specifically, for graft block polymers with flexible backbones, a high graft density could restrict the space available for individual side chains and entire macromolecules to interact and entangle. Graft copolymers with the same graft density but longer side chain length, such as PMen1C-$g_{10\%}$-P*n*BA 4 compared to 3, have an increased tensile toughness.

Interestingly, the mechanical properties of PMen1C-$g_{10\%}$-P*n*BA 3 and 4 are very similar to PLimC, that was functionalized with butyl 3-mercaptopropionate, described first by Hauenstein et al. [16].

3.4 | Electrospinning

The processing of PLimC into non-woven fiber mats via electrospinning was tried unsuccessfully in the past. The stiffness of the polymer chains was assumed to be the reason why no stabile jet could be formed. To test if the addition of side chains could solve this issue, electrospinning was performed with PMen1C_{28}-$g_{10\%}$-P*n*BA_{72} (3). The success of the spinning was at first determined by inspecting the formation of a stabile jet at the tip of the cannula and later confirmed by SEM imaging (Figure 8).

Although fibers are slightly fused together because the solvent could not evaporate fast enough during the spinning process and the residual solvent caused the incoming fibers to be glued onto the previously spun fibers, the fibers are very homogeneous and show no signs of bead formation. At 40 wt%, homogenous fibers were produced even at comparatively high flow rates of 2 mL h^{-1}. The fiber diameter ($d = 3.6 \pm 0.6$ µm) is on the higher end of the spectrum of fiber diameters that are achievable with electrospinning [70]. One possible application for non-wovens of polymers grafted with *n*BA is the utilization as an oil–water-separation material [71–73]. Although other non-wovens made from aliphatic polycarbonates are mostly produced for tissue engineering applications, the biocompatibility of PMen1C_{28}-$g_{10\%}$-P*n*BA_{72} would have to be tested first [74].

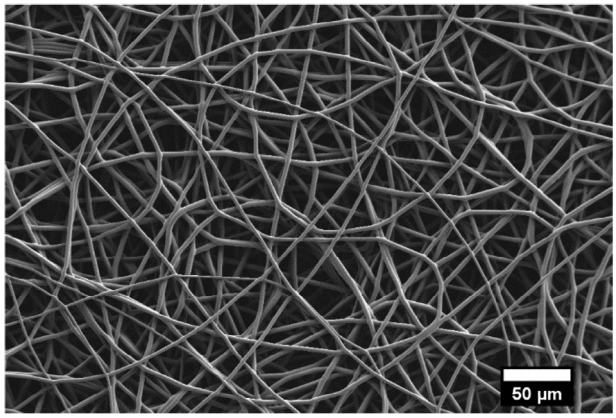

FIGURE 8 | SEM images of an electrospun PMen1C28-g10%-P*n*BA_{72} non-woven. The fiber diameter was determined to be $d = 3.6 \pm 0.6$ µm.

3.5 | Compatibilization of Blends

To test the capability of the graft copolymers to compatibilize immiscible polymer blends of PLimC with P*n*BA, PMen1C_{28}-$g_{10\%}$-P*n*BA_{72} (3) was dissolved alongside neat PLimC and P*n*BA and cast into glass petri dishes to produce blend films. After drying in rotary pump vacuum, the films were observed with light microscopy (Figure S7) and Raman imaging (Figure 9).

The Raman images show that the domains of P*n*BA (depicted in red in Figure 9) are dispersed spheres in a PLimC (blue) matrix. The black dots visible in the second picture (5%) are bubble-shaped drying defects that are also visible in the light microscopy images (Figure S7). A clear trend is visible that the size of P*n*BA droplets is significantly smaller and more evenly distributed with addition of 5% and 10% of the graft copolymer. This trend can be attributed to the interfacial activity of the graft copolymer resulting in lower interfacial tension between the polymer domains (as illustrated in Scheme 3). An increasing concentration of the graft copolymers can therefore stabilize more interfacial surface area and lead to smaller droplets in the matrix. Additionally, the physical crosslinking of the side chains of the graft copolymer and the homopolymer chains facilitates the stabilization of smaller domain sizes [37, 75].

Tensile testing was subsequently used to confirm the ability of the graft copolymers to improve the mechanical properties of PLimC by compatibilizing the blend. Additionally, PMen1C_{28}-$g_{10\%}$-P*n*BA_{72} (3) was solvent blended with PLimC to test its ability as a toughening agent. Representative stress-strain curves are shown in Figure 10.

The neat PLimC displays brittle failure with an elongation at break of $\varepsilon_b = 7\%$ and a toughness of $U_T = 2.4$ MJ m^{-3}. Although the brittle behavior of PLimC is known in literature, these values are rather low compared to previous tensile testing results in our group ($\varepsilon_b = 15\%$) [9]. The difference may stem from the fact that Hauenstein et al. used hot-pressed samples, which results in denser material than solvent casting. With the addition of 10% PMen1C_{28}-$g_{10\%}$-P*n*BA_{72} (3) to PLimC, the elongation at break was increased to $\varepsilon_b = 31\%$, and toughness was improved to $U_T = 12.3$ MJ m^{-3}, whereas the elastic modulus ($E = 1320$ MPa) was not changed. The same trend could be observed for the

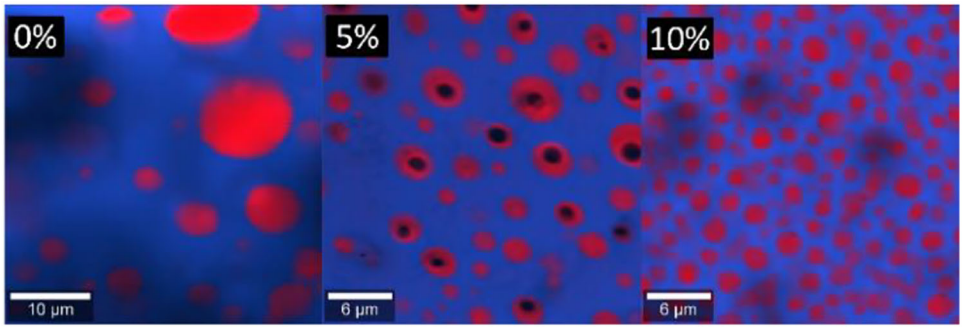

FIGURE 9 | Investigation of the effect of graft copolymer on phase behavior in PLimC/P*n*BA/graft copolymer-blends with 0% (80:20:0), 5% (76:19:5), 10% (72:18:10) graft copolymer content using Raman imaging (PLimC (blue); P*n*BA (red)).

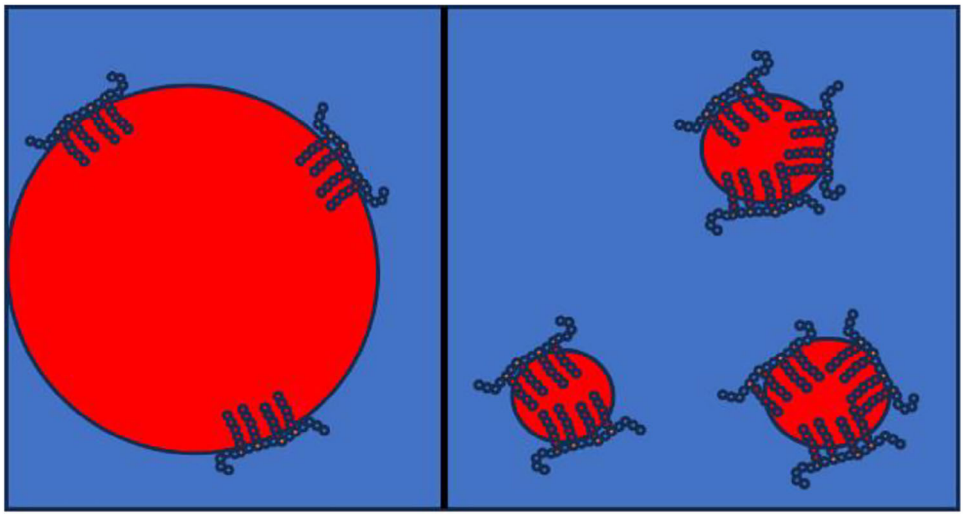

SCHEME 3 | Schematic illustration of the influence of graft copolymer concentration on domain size in an immiscible polymer blend (left side: low graft copolymer concentration; right side: high graft copolymer concentration).

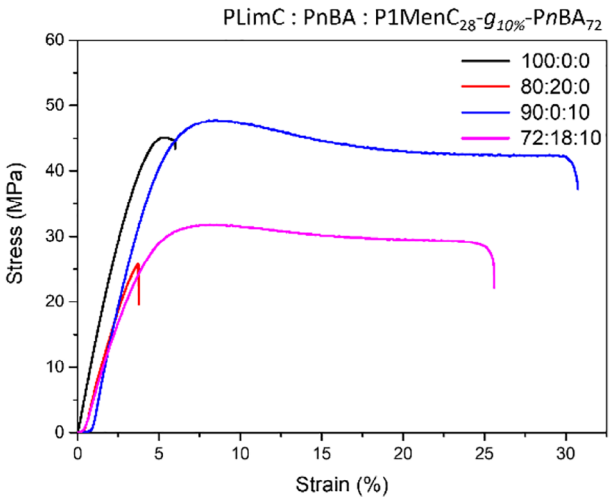

FIGURE 10 | Investigation of the mechanical behavior of samples with different side-chain lengths with fixed backbone length and side-chain composition ((blue; 31%; 9.5 MJ m^{-3}); (black; 7%; 2.4 MJ m^{-3}); (red; 4%; 1.3 MJ m^{-3}); (pink; 26%; 6.9 MJ m^{-3})).

PLimC-P*n*BA-Blend, as the blend without compatibilizer displayed a low elongation at break of $\varepsilon_b = 4\%$ and a toughness of $U_T = 0.5$ MJ m^{-3}, whereas the addition of the graft copolymer 3 increased the elongation at break to $\varepsilon_b = 26\%$ and a toughness of $U_T = 6.9$ MJ m^{-3}. In both cases the blend has decreased the tensile strength compared to neat PLimC; however, addition of the graft copolymer shows a moderate increase of the tensile strength. These results indicate that the addition of the graft copolymer leads to the formation of domains of both homopolymers with graft copolymers at the interfaces, which serve as effective physical cross-links [37]. The addition of the graft copolymer to PLimC seems to allow the PLimC chains to flow more freely during plastic deformation.

4 | Conclusion

In this work, we present a new method to tailor polymer graft density and composition of bio-based graft copolymers, building off our previous work on bio-based copolycarbonates with tailored functionality [56]. We have shown that bio-based graft copolymers PMen1C-*g*-P*n*BA with tailored graft densities between 4 and 33 mol% and narrow molecular weight distribution are accessible

by grafting from P(Men1C-*ran*-LimC) with a PLimC content of 4–33 mol%, employing ATRP after previous functionalization of the exocyclic double bonds of the copolycarbonates. PMen1C-*g*-P*n*BA shows tunable mechanical properties. By variation of P*n*BA content and graft density, the tensile strength was changed from 34 to 1 MPa, whereas elongation changed from 67% to 500%, respectively. PMen1C-*g*-P*n*BA with a graft density of 10% was chosen for all further experiments as it promised a good balance of properties. By producing non-wovens via electrospinning, the possible application as a fiber material was demonstrated. The graft copolymer was successful in compatibilizing blends of PLimC and P*n*BA, as was demonstrated using Raman imaging to investigate the domain sizes and mechanical testing. Finally, the use as toughening agents for PLimC was tested. The addition of the graft copolymer significantly increased the elongation at break while maintaining the Young's modulus, tensile strength, and other beneficial properties of PLimC, such as the high transparency. This work therefore demonstrates the possibility to tune the properties of PLimC to fit a variety of commercial applications, thereby making it possible to replace fossil-based plastics that are currently on the market. PLimC holds significant potential for applications in greenhouse windows and energy-efficient buildings, where its high transparency, selective gas permeability, and enhanced toughness—achieved through the incorporation of the aforementioned graft copolymers—offer distinct advantages [12]. Additionally, with the new possibility of electrospinning, PLimC copolymers could be utilized in the development of bio-based filtration systems. As a next step, the presented graft copolymerization could be scaled up and compounded with PLimC and P*n*BA to test if the blend with compatibilizer and toughening of PLimC shows similar improvement compared to solvent blending. The concept of graft copolymerization could also be applied to other bio-based monomers. Instead of functionalization with BiB for ATRP, the pendant OH-groups can be used for the preparation of graft copolymers employing ring-opening polymerization of lactones and lactides.

Author Contributions

Marcel Höferth: writing– original draft, investigation, methodology, writing– review and editing, conceptualization, data curation. **Holger Schmalz**: conceptualization, writing– review and editing, data curation. **Andreas Greiner**: conceptualization, funding acquisition, writing– review and editing, supervision, project administration, resources.

Acknowledgments

Financial support by German Research Foundation (DFG, GR 972/59-1). The authors would like to thank Rika Schneider for the SEC measurements, Roman Schaller for MALDI-TOF MS measurement, Markus Hund and the KeyLab "Surface and Interface Characterization" for AFM measurements and the KeyLab "Synthesis and Molecular Characterization" of the Bavarian Polymer Institute (BPI) for support.

Open access funding enabled and organized by Projekt DEAL.

Conflicts of Interest

The authors declare no conflicts of interest.

Data Availability Statement

The authors have nothing to report.

References

1. R. Mülhaupt, "Green Polymer Chemistry and Bio-Based Plastics: Dreams and Reality," *Macromolecular Chemistry and Physics* 214 (2013): 159–174.

2. R. M. Cywar, N. A. Rorrer, C. B. Hoyt, G. T. Beckham, and E. Y.-X. Chen, "Bio-Based Polymers With Performance-Advantaged Properties," *Nature Reviews Materials* 7 (2022): 83–103.

3. J.-G. Rosenboom, R. Langer, and G. Traverso, "Bioplastics for a Circular Economy," *Nature Reviews Materials* 7 (2022): 117–137.

4. F. M. Haque, J. S. A. Ishibashi, C. A. L. Lidston, et al., "Defining the Macromolecules of Tomorrow Through Synergistic Sustainable Polymer Research," *Chemical Reviews* 122 (2022): 6322–6373.

5. Y. Yin and M. W. Woo, "Transitioning of Petroleum-Based Plastic Food Packaging to Sustainable Bio-Based Alternatives," *Sustainable Food Technology* 2 (2024): 548–566.

6. M. Firdaus and M. A. R. Meier, "Renewable Polyamides and Polyurethanes Derived From Limonene," *Green Chemistry* 15 (2013): 370–380.

7. M. M. Kleybolte, C. P. Vogt, and M. Winnacker, "High Precision Tuning of Limonene Polyamide via Side-Chain Functionalization for Specialized Applications," *Macromolecular Chemistry and Physics* 2500021 (2025): 1–8.

8. C. M. Byrne, S. D. Allen, E. B. Lobkovsky, and G. W. Coates, "Alternating Copolymerization of Limonene Oxide and Carbon Dioxide," *Journal of the American Chemical Society* 126 (2004): 11404–11405.

9. O. Hauenstein, M. Reiter, S. Agarwal, B. Rieger, and A. Greiner, "Bio-Based Polycarbonate From Limonene Oxide and CO_2 With High Molecular Weight, Excellent Thermal Resistance, Hardness and Transparency," *Green Chemistry* 18 (2016): 760–770.

10. S. D. Allen, D. R. Moore, E. B. Lobkovsky, and G. W. Coates, "Structure and Reactivity of Mono-and Dinuclear Diiminate Zinc Alkyl Complexes," *Journal of Organometallic Chemistry* 683 (2003): 137–148.

11. C. Li, J. Madsen, S. P. Armes, and A. L. Lewis, "A New Class of Biochemically Degradable, Stimulus-Responsive Triblock Copolymer Gelators," *Angewandte Chemie International Edition* 45 (2006): 3510–3513.

12. O. Hauenstein, M. M. Rahman, M. Elsayed, et al., "Biobased Polycarbonate as a Gas Separation Membrane and "Breathing Glass" for Energy Saving Applications," *Advanced Materials Technologies* 2 (2017): 1700026.

13. C. Li, R. J. Sablong, R. A. T. M. van Benthem, and C. E. Koning, "Unique Base-Initiated Depolymerization of Limonene-Derived Polycarbonates," *ACS Macro Letters* 6 (2017): 684–688.

14. A. Durkin, I. Taptygin, Q. Kong, et al., "Scale-Up and Sustainability Evaluation of Biopolymer Production From Citrus Waste Offering Carbon Capture and Utilisation Pathway," *ChemistryOpen* 8 (2019): 668–688.

15. D. Zhang, E. A. Del Rio-Chanona, J. L. Wagner, and N. Shah, "Life Cycle Assessments of Bio-Based Sustainable Polylimonene Carbonate Production Processes," *Sustainable Production and Consumption* 14 (2018): 152–160.

16. O. Hauenstein, S. Agarwal, and A. Greiner, "Bio-Based Polycarbonate as Synthetic Toolbox," *Nature Communications* 7 (2016): 11862.

17. C. Li, S. van Berkel, R. J. Sablong, and C. E. Koning, "Post-Functionalization of Fully Biobased Poly(Limonene Carbonate)s: Synthesis, Characterization and Coating Evaluation," *European Polymer Journal* 85 (2016): 466–477.

18. N. Kindermann, À. Cristòfol, and A. W. Kleij, "Access to Biorenewable Polycarbonates With Unusual Glass-Transition Temperature (Tg) Modulation," *ACS Catalysis* 7 (2017): 3860–3863.

19. A. K. van der Vegt and L. Govaert, *Polymeren*. Van *keten tot kunststof* (VSSD, 2009).

20. G. Wypych, *Handbook of Polymers* (Elsevier, 2012).

21. S. Neumann, L.-C. Leitner, H. Schmalz, S. Agarwal, and A. Greiner, "Unlocking the Processability and Recyclability of Biobased Poly

(Limonene Carbonate)," *ACS Sustainable Chemistry & Engineering* 8 (2020): 6442–6448.

22. X. Zhang, Y. Li, J. M. Hankett, and Z. Chen, "The Molecular Interfacial Structure and Plasticizer Migration Behavior of "Green" Plasticized Poly (Vinyl Chloride)," *Physical Chemistry Chemical Physics* 17 (2015): 4472–4482.

23. M. W. Halloran, J. A. Nicell, R. L. Leask, and M. Marić, "Small Molecule Plasticizers for Improved Migration Resistance: Investigation of Branching and Leaching Behaviour in PVC Blends," *Materials Today Communications* 29 (2021): 102874.

24. F. Jiang, Z. Wang, Y. Qiao, Z. Wang, and C. Tang, "A Novel Architecture Toward Third-Generation Thermoplastic Elastomers by a Grafting Strategy," *Macromolecules* 46 (2013): 4772–4780.

25. M. Hayashi, K. Shibata, and S. Nobukawa, "Advantage of Graft Architecture With a Flexible Main Chain for Implantation of Ductile Nature Into Brittle Amorphous Acrylic Glass," *Polymer* 236 (2021): 124316.

26. P. Alagi, G. Zapsas, N. Hadjichristidis, S. C. Hong, Y. Gnanou, and X. Feng, "All-Polycarbonate Graft Copolymers With Tunable Morphologies by Metal-Free Copolymerization of CO_2 With Epoxides," *Macromolecules* 54 (2021): 6144–6152.

27. D. Neugebauer, Y. Zhang, T. Pakula, S. S. Sheiko, and K. Matyjaszewski, "Densely-Grafted and Double-Grafted PEO Brushes via ATRP. A Route to Soft Elastomers," *Macromolecules* 36 (2003): 6746–6755.

28. T. Pakula, Y. Zhang, K. Matyjaszewski, et al., "Molecular Brushes as Super-Soft Elastomers," *Polymer* 47 (2006): 7198–7206.

29. B. Lee, M. J. Maher, H. J. Schibur, M. A. Hillmyer, and F. S. Bates, "Toughening Polylactide With Graft-Block Polymers," *ACS Applied Polymer Materials* 4 (2022): 3408–3416.

30. N. Z. Tomić and A. D. Marinković, *Compatibilization of Polymer Blends* (Elsevier, 2020).

31. R. V. Barbosa, M. A. R. Moraes, A. S. Gomes, and B. G. Soares, "Eva-Based Graft Copolymers as Compatibilizing Agents for Polymer Blends," *Journal of Macromolecular Science, Part A: Pure and Applied Chemistry* 32 (1995): 663–669.

32. L. Caporaso, N. Iudici, and L. Oliva, "A Novel Route to Graft-Copolymers With Tailored Structures for the Compatibilization of Polymeric Blend," *Macromolecular Symposia* 234 (2006): 42–50.

33. D. Chen, H. Wang, and Y. Li, "Reactive Compatibilization: Formation of Double-Grafted Copolymers by In Situ Binary Grafting and Their Compatibilization Effect," *ACS Applied Materials & Interfaces* 9 (2017): 33091–33099.

34. I. A. Gianoglio Pantano, M. Asteasuain, C. Sarmoria, and A. Brandolin, "Graft Copolymers for Blend Compatibilization: Mathematical Modeling of the Grafting Process," *Macromolecular Reaction Engineering* 6 (2012): 406–418.

35. H. K. Jeon, B. J. Feist, S. B. Koh, K. Chang, C. W. Macosko, and R. P. Dion, "Reactively Formed Block and Graft Copolymers as Compatibilizers for Polyamide 66/PS Blends," *Polymer* 45 (2004): 197–206.

36. K. Klimovica, S. Pan, T.-W. Lin, et al., "Compatibilization of i PP/HDPE Blends With PE-*g*-i PP Graft Copolymers," *ACS Macro Letters* 9 (2020): 1161–1166.

37. D. G. Peiffer and M. Rabeony, "Physical Properties of Model Graft Copolymers and Their Use as Blend Compatibilizers," *Journal of Applied Polymer Science* 51 (1994): 1283–1289.

38. Y. Xu, C. M. Thurber, T. P. Lodge, and M. A. Hillmyer, "Synthesis and Remarkable Efficacy of Model Polyethylene-Graft-Poly(Methyl Methacrylate) Copolymers as Compatibilizers in Polyethylene/Poly(Methyl Methacrylate) Blends," *Macromolecules* 45 (2012): 9604–9610.

39. C.-L. Zhang, L.-F. Feng, X.-P. Gu, S. Hoppe, and G.-H. Hu, "Efficiency of Graft Copolymers as Compatibilizers for Immiscible Polymer Blends," *Polymer* 48 (2007): 5940–5949.

40. C.-L. Zhang, L.-F. Feng, X.-P. Gu, S. Hoppe, and G.-H. Hu, "Blend Composition Dependence of the Compatibilizing Efficiency of Graft Copolymers for Immiscible Polymer Blends," *Polymer Engineering and Science* 50 (2010): 2243–2251.

41. C. Zhang, C. Man, Y. Pan, W. Wang, L. Jiang, and Y. Dan, "Toughening of Polylactide With Natural Rubber Grafted With Poly(Butyl Acrylate)," *Polymer International* 60 (2011): 1548–1555.

42. Y. Teramoto, M. Yoshioka, N. Shiraishi, and Y. Nishio, "Plasticization of Cellulose Diacetate by Graft Copolymerization of ε-Caprolactone and Lactic Acid," *Journal of Applied Polymer Science* 84 (2002): 2621–2628.

43. W. Liu, Y. Liu, G. Zeng, R. Liu, and Y. Huang, "Coil-to-Rod Conformational Transition and Single Chain Structure of Graft Copolymer by Tuning the Graft Density," *Polymer* 53 (2012): 1005–1014.

44. D. Ghosh and S. Agarwal, "Synthesis and Degradation Study of Graft Copolymers of Poly(Limonene Carbonate)," *Polymer Chemistry* 14 (2023): 4626–4635.

45. D. Skoulas, A. Tolentino, and A. W. Kleij, "Controlled Synthesis of Bioderived Poly(limonene carbonate) Oligolysine Hybrid Macromolecules," *ACS Macro Letters* 13, no. 10 (2024): 1332–1337.

46. Y. Inoue, T. Matsugi, N. Kashiwa, and K. Matyjaszewski, "Graft Copolymers From Linear Polyethylene via Atom Transfer Radical Polymerization," *Macromolecules* 37 (2004): 3651–3658.

47. A. Gregory and M. H. Stenzel, "Complex Polymer Architectures via RAFT Polymerization: From Fundamental Process to Extending the Scope Using Click Chemistry and Nature's Building Blocks," *Progress in Polymer Science* 37 (2012): 38–105.

48. R. G. Lopez, F. D'Agosto, and C. Boisson, "Synthesis of Well-Defined Polymer Architectures by Successive Catalytic Olefin Polymerization and Living/Controlled Polymerization Reactions," *Progress in Polymer Science* 32 (2007): 419–454.

49. C. Feng, Y. Li, D. Yang, J. Hu, X. Zhang, and X. Huang, "Well-Defined Graft Copolymers: From Controlled Synthesis to Multipurpose Applications," *Chemical Society Reviews* 40 (2011): 1282–1295.

50. N. Ding, B. Shentu, P. Pan, G. Shan, Y. Bao, and Z. Weng, "Synthesis and Crystallization of Poly(Vinyl Acetate)-g-Poly(L-Lactide) Graft Copolymer With Controllable Graft Density," *Industrial & Engineering Chemistry Research* 52 (2013): 12897–12905.

51. J. Zhang, D. K. Schneiderman, T. Li, M. A. Hillmyer, and F. S. Bates, "Design of Graft Block Polymer Thermoplastics," *Macromolecules* 49 (2016): 9108–9118.

52. A. B. Chang, T.-P. Lin, N. B. Thompson, et al., "Design, Synthesis, and Self-Assembly of Polymers With Tailored Graft Distributions," *Journal of the American Chemical Society* 139 (2017): 17683–17693.

53. T.-P. Lin, A. B. Chang, S.-X. Luo, H.-Y. Chen, B. Lee, and R. H. Grubbs, "Effects of Grafting Density on Block Polymer Self-Assembly: From Linear to Bottlebrush," *ACS Nano* 11 (2017): 11632–11641.

54. T. Liu, R. Parekh, P. Mocny, et al., "Tailored PVDF Graft Copolymers via ATRP as High-Performance NCM811 Cathode Binders," *ACS Materials Letters* 5 (2023): 2594–2603.

55. J. Geschwind, F. Wurm, and H. Frey, "From CO_2-Based Multifunctional Polycarbonates With a Controlled Number of Functional Groups to Graft Polymers," *Macromolecular Chemistry and Physics* 214 (2013): 892–901.

56. M. Höferth, H. Schmalz, and A. Greiner, "Bio-Based, Random Terpolymers With Defined Functionality Based on Poly(Limonene Carbonate-Ran-Menth-1-Ene Carbonate)," *Polymer Chemistry* 15 (2024): 1522–1529.

57. K. Matyjaszewski, Y. Nakagawa, and C. Jasieczek, "Polymerization of n-Butyl Acrylate by Atom Transfer Radical Polymerization. Remarkable Effect of Ethylene Carbonate and Other Solvents," *Macromolecules* 31 (1998): 1535–1541.

58. S. V. Arehart and K. Matyjaszewski, "Atom Transfer Radical Copolymerization of Styrene and n-Butyl Acrylate," *Macromolecules* 32 (1999): 2221–2231.

59. X. Pan, S. Lathwal, S. Mack, J. Yan, S. R. Das, and K. Matyjaszewski, "Automated Synthesis of Well-Defined Polymers and Biohybrids by Atom Transfer Radical Polymerization Using a DNA Synthesizer," *Angewandte Chemie International Edition* 56 (2017): 2740–2743.

60. F. Lorandi, Y. Wang, M. Fantin, and K. Matyjaszewski, "Ab Initio Emulsion Atom-Transfer Radical Polymerization," *Angewandte Chemie International Edition* 57 (2018): 8270–8274.

61. S. G. Roos, A. H. E. Müller, and K. Matyjaszewski, "Copolymerization of n-Butyl Acrylate With Methyl Methacrylate and PMMA Macromonomers: Comparison of Reactivity Ratios in Conventional and Atom Transfer Radical Copolymerization," *Macromolecules* 32 (1999): 8331–8335.

62. A. Oudshoorn, L. A. van der Wielen, and A. J. Straathof, "Techno-Economic Analysis of Butanol Production From Lignocellulosic Biomass by Concentrated Acid Pretreatment and Hydrolysis Plus Continuous Fermentation," *Biochemical Engineering Journal* 48 (2009): 99–103.

63. A. Niesbach, P. Lutze, and A. Górak, "Reactive Distillation for Production of n-Butyl Acrylate From Bio-Based Raw Materials," *Computer Aided Chemical Engineering* 32 (2013): 223–228.

64. J. G. H. Hermens, A. Jensma, and B. L. Feringa, "Highly Efficient Biobased Synthesis of Acrylic Acid," *Angewandte Chemie International Edition* 61 (2022): 202112618.

65. O. Colombani, M. Ruppel, F. Schubert, H. Zettl, D. V. Pergushov, and A. H. E. Müller, "Synthesis of Poly(n-Butyl Acrylate)-Block-Poly(Acrylic Acid) Diblock Copolymers by ATRP and Their Micellization in Water," *Macromolecules* 40 (2007): 4338–4350.

66. W. A. Braunecker, N. V. Tsarevsky, A. Gennaro, and K. Matyjaszewski, "Thermodynamic Components of the Atom Transfer Radical Polymerization Equilibrium: Quantifying Solvent Effects," *Macromolecules* 42 (2009): 6348–6360.

67. S. Özlem and J. Hacaloglu, "Thermal Degradation of Poly(n-Butyl Methacrylate), Poly(n-Butyl Acrylate) and Poly(t-Butyl Acrylate)," *Journal of Analytical and Applied Pyrolysis* 104 (2013): 161–169.

68. P. Schön, K. Bagdi, K. Molnár, P. Markus, B. Pukánszky, and G. J. Vancso, "Quantitative Mapping of Elastic Moduli at the Nanoscale in Phase Separated Polyurethanes by AFM," *European Polymer Journal* 47 (2011): 692–698.

69. A. Rasmont, P. Leclère, C. Doneux, et al., "Microphase Separation at the Surface of Block Copolymers, as Studied With Atomic Force Microscopy," *Colloids and Surfaces B: Biointerfaces* 19 (2000): 381–395.

70. B. Cramariuc, R. Cramariuc, R. Scarlet, L. R. Manea, I. G. Lupu, and O. Cramariuc, "Fiber Diameter in Electrospinning Process," *Journal of Electrostatics* 71 (2013): 189–198.

71. F. Yuan, J. Wei, E. Tang, and K. Zhao, "Synthesis of Butyl Acrylate Grafted Polypropylene Fibre and Its Applications on Oil-Adsorption in Floating Water," *e-Polymers* 9 (2009): 1–8.

72. N. Xu, J. Cao, and Y. Lu, "The Electrospinning of the Copolymer of Styrene and Butyl Acrylate for Its Application as Oil Absorbent," *SpringerPlus* 5 (2016): 1383.

73. P.-X. Guo, X.-G. Wang, M.-Q. Yang, J.-X. Wang, and F.-J. Meng, "Preparation and Oil Adsorption of Cellulose-Graft-Poly(Butyl Acrylate-N,N′-Methylene Bisacrylamide)," *Materials* 17 (2024): 1–17.

74. P. Wei, G. A. Bhat, and D. J. Darensbourg, "Enabling New Approaches: Recent Advances in Processing Aliphatic Polycarbonate-Based Materials," *Angewandte Chemie International Edition* 62 (2023): 202307507.

75. R. Schaller, M. Schmidt, K. Schweimer, and H. Schmalz, "Patchy Stereocomplex Micelles as Efficient Compatibilizers for Polymer Blends," *Polymer Chemistry* 15 (2024): 3100–3112.

Supporting Information

Additional supporting information can be found online in the Supporting Information section.

Supporting file 1: ejlt70037-sup-0001-SuppMat.docx